The Journal of Chemical Physics

How symmetry-breaking can amplify the magnetosensitivity of dipolarly coupled *n*-radical systems

Cite as: J. Chem. Phys. **154**, 094101 (2021); https://doi.org/10.1063/5.0041552
Submitted: 24 December 2020 • Accepted: 02 February 2021 • Published Online: 01 March 2021

Robert H. Keens, Chris Sampson and Daniel R. Kattnig

AIP Publishing

The Journal of Chemical Physics ARTICLE scitation.org/journal/jcp

How symmetry-breaking can amplify the magnetosensitivity of dipolarly coupled *n*-radical systems

Cite as: J. Chem. Phys. 154, 094101 (2021); doi: 10.1063/5.0041552
Submitted: 24 December 2020 • Accepted: 2 February 2021 •
Published Online: 1 March 2021

Robert H. Keens, Chris Sampson, and Daniel R. Kattnig[a)]

AFFILIATIONS

Living Systems Institute and Department of Physics, University of Exeter, Stocker Road, Exeter, Devon EX4 4QD, United Kingdom

[a)]**Author to whom correspondence should be addressed:** D.R.Kattnig@exeter.ac.uk

ABSTRACT

In systems of more than two reactive radicals, the radical recombination probability can be magnetosensitive due to the mere effect of the inter-radical electron–electron dipolar coupling. Here, we demonstrate that this principle, previously established for three-radical systems, generalizes to *n*-radical systems. We focus on radical systems in the plane and explore the effects of symmetry, in particular its absence, on the associated magnetic field effects of the recombination yield. We show, by considering regular configurations and slightly distorted geometries, that the breaking of geometric symmetry can lead to an enhancement of the magnetosensitivity of these structures. Furthermore, we demonstrate the presence of effects at low-field that are abolished in the highly symmetric case. This could be important to the understanding of the behavior of radicals in biological environments in the presence of weak magnetic fields comparable to the Earth's, as well as the construction of high-precision quantum sensing devices.

INTRODUCTION

Many theoretical models exist that attempt to describe how magnetism and biology interact. For the domain of low magnetic fields, i.e., fields comparable to the geomagnetic field (≈50 μT) and ranging to a few mT, the most widely accepted premise is that of the Radical Pair Mechanism (RPM).[1–3] The RPM is actualized in the magnetosensitivity of the reaction yields and kinetics of chemical processes involving transient, spin-correlated pairs of radicals.[4] In this model, the magnetic field modulates the coherent interconversion of electronic singlet and triplet states of the radical pair, which is driven by hyperfine interactions with magnetic nuclei in the radicals. The resulting magnetic field effects (MFEs) on chemical reactions are now very well-established.[1,5–8] The RPM has also been in the spotlight recently due to its putative underpinning of a protein-based magnetic compass sense (involving the protein cryptochrome) in various organisms,[9,10] which makes it a central contender of the emerging field of quantum biology.[11,12]

In contrast to the two-radical systems of the classical RPM, larger systems have attracted comparably little attention. Systems of three electron spins have been discussed: in the context of spin catalysis,[13] the chemical Zeno effect,[14,15] and quantum teleportation[16] and as a decoherence pathway.[17] In spin catalysis, the exchange coupling of the radical pair with the spin catalyst is the main interaction motif. As the Zeeman part of the Hamiltonian commutes with the exchange Hamiltonian, this interaction alone cannot produce MFEs. However, mutual exchange coupling can facilitate near level-crossings at certain strengths of an external magnetic field, whereupon hyperfine-driven spin conversion can proceed efficiently[18,19] and may also transmit the effect of a quickly relaxing third radical.[20] A perturbative approach based on a Hubbard–trimer Hamiltonian has been used to show that this additional radical can further enhance the intersystem crossing rate.[21] Quantum teleportation and spin coherence transfer in three-radical systems have actually been realized experimentally.[21,22] Furthermore, the spin-selective reaction of a radical pair with a scavenger radical

has been shown to boost anisotropic magnetic field effects in the geomagnetic field[23] and provide resilience to spin relaxation in one of the radicals of the triad,[15] thereby providing decisive advantages over the classical RPM model of magnetoreception. To the best of the authors' knowledge, such three-radical systems have only been discussed in the biological context in Refs. 15, 16, and 23. These models have however disregarded the effects of electron–electron dipolar (EED) interactions. As we have previously shown by symmetry considerations, the EED interaction alone is sufficient for MFE genesis in systems of three radicals and so clearly should not be neglected in the consideration of biological radical dynamics.[24]

The EED coupling of the electrons is an unavoidable consequence of their intrinsic magnetic moment.[4] As the interaction is averaged to zero for a spherical distribution of inter-radical vectors, it is often neglected for radicals diffusing freely in solution. On the other hand, for immobilized radical systems (such as the radical pairs implicated in models of cryptochrome magnetoreception[25,26]) or radicals diffusing in a reduced dimension (such as peroxyl radicals in a lipid bilayer[27]), they are almost certainly not negligible, as the interaction energy decays only slowly, i.e., by r^{-3}, with inter-radical distance r. Thus, for distances of 1.5 nm (typical for flavin/tryptophan radical pairs in cryptochrome) and 0.7 nm (the contact distance of peroxyl radicals), the interaction amounts to 15 MHz or 150 MHz, respectively, which exceeds the Larmor precession frequency of the free electron in the geomagnetic field (~1.4 MHz for $B = 50\ \mu$T) and often typical hyperfine interaction frequencies (~1 MHz–50 MHz). The mutual compensation of EED and exchange interactions has often been argued to justify neglecting inter-radical interactions in magnetoreceptor systems.[26] However, this simplifying assumption was recently shown to not always be appropriate.[25]

Alternative sources of magnetosensitivity in radical reaction processes have been suggested. We have recently proposed a mechanism, named *D3M*, that highlights the EED coupling as a possible source of MFEs on radical recombination reactions in (partly) ordered, i.e., immobilized, systems of *three* radicals. The mechanism requires that more than two radicals simultaneously interact via the EED interaction, which can be the case even at low radical concentrations due to the slow decay of the dipolar interaction with distance.[24] D3M is distinct from other three-radical effects, such as the chemical Zeno effect and its use for quantum teleportation,[16,22] as it realizes an intrinsic magnetic field-sensitivity independent of hyperfine interactions.[24] The effect has been suggested to explain the putative magnetic field sensitivity of lipid autoxidation,[27] which is characterized by the recombination of radicals for which the hyperfine interaction is small compared to the EED coupling, and to enhance the cryptochrome compass sensitivity by a nonreactive *bystander* radical.[25] These findings are noteworthy insofar as in the RPM the effect of the EED interaction is well known to suppress MFEs in weak magnetic fields by energetically uncoupling the singlet and triplet manifolds, thereby suppressing their coherent coupling. On the other hand, the D3M effects appear to persist in the presence of both hyperfine and exchange interactions.[24,25,27]

Here, we generalize D3M to treat larger systems of n spins, with $n \geq 3$, which we call DnM. To the best of the authors' knowledge, MFEs in systems of more than three radicals have not been studied at all, and it is on these systems that we focus primarily. We have considered three-spin systems as a baseline for the DnM mechanism and build from there to observe new, surprising, and potentially biologically relevant MFEs in these $n \geq 3$ systems.

This manuscript is structured as follows: in model and computation, we generalize the D3M model to DnM, with $n \geq 3$, summarize the pertinent parameters and assumptions of the model, and detail how we solved the Liouville–von Neumann equation for these systems. We also present a qualitative model for DnM based on an equipartitioning argument over accessible states for the case that one radical pair recombines. In Sec. IV, we present the characteristic features of DnM for the selected systems, whereby we focus on planar systems, as inspired in Ref. 27. The core theme is that systems with small geometric irregularities show stronger, more diverse MFEs, including new effects at the low-field, when compared with their counterpart, highly symmetric systems. We first explore regular polygons, and their distorted counterparts, and then move on to the special case of the linear chain. In the main text, we focus on the four-spin configuration, with further results for three to six spins shown in Figs. S4–S7 of the supplementary material. Finally, we discuss our results, their significance, and their potential applications to various areas of quantum biology.

MODEL AND COMPUTATION

Here, we work from the premise of the recently proposed *D3M* mechanism[24] and extend it to *DnM* with $n > 3$, where n is the number of interacting radicals. We consider the effect of the oft-neglected electron–electron dipolar interaction as the main contributor to MFEs. The DnM Hamiltonian (in angular frequency units) is thus

$$\begin{aligned}\hat{H} &= \hat{H}_{dd} + \hat{H}_{ex} + \hat{H}_{Ze} \\ &= \sum_{i<j}^{N} \hat{\mathbf{S}}_i \cdot \mathbf{D}_{i,j} \cdot \hat{\mathbf{S}}_j - \sum_{i<j}^{N} J_{i,j}\left(\frac{1}{2} + 2\hat{\mathbf{S}}_i \cdot \hat{\mathbf{S}}_j\right) + \gamma \mathbf{B} \cdot \sum_{i}^{N} \hat{\mathbf{S}}_i, \end{aligned} \quad (1)$$

where the individual summands account for the electron–electron dipolar ($\hat{H}_{dd}$), exchange ($\hat{H}_{ex}$), and Zeeman interactions ($\hat{H}_{Ze}$). $\mathbf{B}$ denotes the applied magnetic field, B denotes its intensity, and $\gamma = \frac{g\mu_B}{\hbar}$, with g denoting the electron g-factor. The Larmor precession frequency is $\gamma B/2\pi$. Here, we have assumed that the Zeeman interaction is isotropic and identical for all radicals on account of our focus on the MFEs of organic radicals in weak magnetic fields, i.e., $g \approx 2$; the anisotropies of g are negligible for moderate B.

The dipolar interaction Hamiltonian, calculated within the point-dipole approximation, is of the following form:

$$\hat{\mathbf{S}}_i \cdot \mathbf{D}_{i,j} \cdot \hat{\mathbf{S}}_j = d_{i,j}(r_{i,j})\left[\hat{\mathbf{S}}_i \cdot \hat{\mathbf{S}}_j - 3\left(\hat{\mathbf{S}}_i \cdot \mathbf{e}_{i,j}\right)\left(\hat{\mathbf{S}}_j \cdot \mathbf{e}_{i,j}\right)\right], \quad (2)$$

where $\mathbf{e}_{i,j}$ is a unit vector in the direction of the vector connecting radical i and j at distance r_{ij} and

$$d(r_{ij}) = \frac{\mu_0 g^2 \mu_B^2}{4\pi\hbar r_{ij}^3}. \quad (3)$$

Finally, the exchange Hamiltonian is

$$\hat{H}_{ex} = -\sum_{i<j}^{N} J(|\mathbf{r}_{ij}|)\left(\frac{1}{2} + 2\hat{\mathbf{S}}_i \cdot \hat{\mathbf{S}}_j\right), \tag{4}$$

where $J(|\mathbf{r}_{ij}|)$ is the exchange coupling constant between the ith and jth radical.

We consider pairwise recombination in our model. Making use of the Haberkorn approach,[28] this gives rise to a master equation of the following form:

$$\frac{d\hat{\rho}}{dt} = -i\left[\hat{H}, \hat{\rho}\right] - \left[\hat{K}, \hat{\rho}\right]_+ - k_e\hat{\rho}, \tag{5}$$

where the bracket $[]_+$ denotes the anti-commutator and the recombination operator $\hat{K}$ is given by

$$\hat{K} = \sum_{i<j} \frac{k_S(|\mathbf{r}_{ij}|)}{2} \hat{P}_{i,j}^{(S)}, \tag{6}$$

where $k_S(|\mathbf{r}|_{ij})$ represents the singlet recombination rate constant between radicals i and j. Here, $\hat{P}_{i,j}^{(S)}$ is the projection operator onto the singlet subspace of radicals i and j, which can be written in the following form:

$$\hat{P}_{i,j}^{(S)} = \frac{1}{4}\hat{1} - \hat{\mathbf{S}}_i \cdot \hat{\mathbf{S}}_j. \tag{7}$$

Equation (5) allows us to formulate the time-dependent density matrix as

$$\hat{\rho}(t) = \exp(-k_e t)\exp(-i\hat{A}t)\hat{\rho}(0)\exp(i\hat{A}^{\dagger}t), \tag{8}$$

where k_e is the escape rate constant and $\hat{A}$ is a non-Hermitian effective Hamiltonian operator that accounts for coherent evolution and recombination,

$$\hat{A} = \hat{H} - i\hat{K}. \tag{9}$$

In Eq. (8), we use an initial density matrix, $\hat{\rho(0)} = \hat{1}/2^n$, proportional to the identity matrix to simulate a random initial spin configuration.

The reaction yields can be evaluated by finding the eigenvalues and eigenvectors of the effective Hamiltonian, denoted by λ and T, respectively, and then computing the time-integrated density matrix from

$$\int_0^{\infty} \rho_{ij}(t) = \sum_{k,l,m,n} T_{i,k}T_{k,l}^{-1}\rho_{l,m}(0)(T^{-1})_{k,m}^{*}T_{j,n}^{*}\frac{1}{k_e + i(\lambda_k - \lambda_k^{*})}, \tag{10}$$

where subscript indices denote matrix elements. Taking these quantities together, we calculate the singlet recombination yield

$$\varphi_S = 2Tr\left[\int \hat{\rho}(t)dt\hat{K}\right], \tag{11}$$

which we use to quantify the effect that the applied magnetic field has on the recombination yield by defining the magnetic field effect (MFE) as

$$\chi_S(B) = \frac{\varphi_S(B) - \varphi_S(0)}{\varphi_S(0)}, \tag{12}$$

where $\varphi_S(B)$ is the singlet yield at an applied field of intensity B and $\varphi_S(0)$ is the same quantity at zero-field.

In general, the MFE depends on the geometry of the recombining radicals due to the distance-dependence of the EED interaction and of the parameters k_S and J. For the latter parameters, both are assumed to have an exponential fall-off in keeping with the typical distance dependence of the electron coupling matrix element dictating electron transfer reactions. These take the following form:

$$k_S(|\mathbf{r}_{ij}|) = k_{S,0}\exp(-\beta(|\mathbf{r}_{ij}| - 2R)) \tag{13}$$

and

$$J(|\mathbf{r}_{ij}|) = J_0\exp(-\beta(|\mathbf{r}_{ij}| - 2R)). \tag{14}$$

In both of the above, we have used the same decay rate, $\beta = 1.4$ Å^{-1}. R is a reference distance, which can be interpreted as the radical radius; here, it was fixed at 7.5 Å. For $r_{ij} = 2R$, $d_{1,2}$ thus was 15 MHz. $k_{S,0}^{-1}$ was 200 ns, and k_e^{-1} was 1 μs. B was varied on a logarithmic scale between 0.001 mT and 1000 mT, and it was perpendicular to the plane of the reacting radicals. We have implemented solving Eq. (5) in Python, whereby we rely on an MKL-based implementation for solving the eigenvalue problem for non-Hermitian matrices. The computer code used is a generalization of that described in Ref. 24 for more than three-radicals. It covers an arbitrary number of radicals including all interactions named above, in addition to hyperfine interactions, if desirable. Being based on the eigenvalue decomposition of the effective Hamiltonian, it aims at systems of moderate size. Larger systems could, in principle, be treated by a Monte Carlo wavefunction approach[29] but are beyond this presentation.

A QUALITATIVE MODEL OF MAGNETOSENSITIVITY OF A RADICAL PAIR RECOMBINING IN AN ENVIRONMENT OF RADICALS

We want to offer a qualitative model that accounts for the MFEs of the kind discussed here. To this end, consider a pair of electron spins (radicals devoid of hyperfine interactions) poised to undergo a spin-selective recombination reaction in the singlet state. Assume further that a reactive pair of spins interacts with an environment of radicals, which are assumed unreactive, e.g., due to being too distant to react or intrinsically unreactive. All $n = \ell + 2$ radicals are assumed to interact via EED interactions. Assuming that a reactive radical pair is born in the singlet configuration, we ask with which probability it will still be in the singlet configuration at the moment of reaction. If the radical system is long-lived, the recombination reaction slow and decoherent channels are insignificant, we can assume that in the first approximation, the singlet probability upon

recombination is obtained by equipartitioning the initial population over all accessible spin states. In weak magnetic fields for a random, i.e., asymmetric, geometric arrangement of spins with equally arbitrary magnetic field orientation, all spin states will be coupled by the EED interaction. Consequently, the long-time singlet probability will be $\frac{1}{4}$. This also applies to an arbitrary, i.e., non-special, spin configuration in a plane. While here the Hamiltonian can be decomposed into two blocks (assume that the plane is perpendicular to the z-direction; the EED direction then only couples states with a difference of total spin projection of $\Delta M = \pm 2$, giving rise to two blocks), the singlet probability still turns out as $\frac{1}{4}$. In high magnetic fields, on the other hand, the Zeeman interaction is dominant and states of different total spin projection $M = \sum_i m_i$ are energetically separated such that no spin mixing, i.e., singlet state redistributing, is possible between these states (while it remains intact within). The number of ways by which the additional spins (with index 3 to n) can produce a combined spin projection of $M_{3,\ldots,n} = \sum_{i=3}^{n} m_i$ is $\binom{\ell}{M_{3,\ldots,n}+\frac{\ell}{2}}$. A particular M can then be realized by combining the singlet state of the reactive radical pair with the $M_{3,\ldots,n} = M$ states of radical 3 to n, combining the T_0 state of the reactive radical pair with the $M_{3,\ldots,n} = M$ states of radical 3 to n, combining the T_+ state of the reactive radical pair with the $M_{3,\ldots,n} = M - 1$ states of radical 3 to n, or combining the T_- state of the reactive radical pair with the $M_{3,\ldots,n} = M + 1$ states of radical 3 to n. Thus, the number of states of projection M is

$$s(k) = \binom{\ell}{k-1} + 2\binom{\ell}{k} + \binom{\ell}{k+1}, \tag{15}$$

where $k = M_{3,\ldots,n} + \frac{\ell}{2}$. As the singlet configuration of spins 1 and 2 with projection specified by k is initially generated in $\binom{\ell}{k}$ ways, and the total number of initial singlet states is 2^ℓ and only the singlet pairs recombine, the singlet fraction in the equilibrated system is

$$\begin{aligned} p_{S\to S}(\text{high field}) &= \frac{1}{2^\ell}\sum_{k=0}^{\ell}\frac{1}{s(k)}\binom{\ell}{k}^2 \\ &= \frac{\ell^2+3\ell+4}{4(\ell^2+3\ell+2)} \\ &= \frac{1}{4} + \frac{1}{2n(n-1)}. \end{aligned} \tag{16}$$

Finally, the magnetic field effect is

$$\begin{aligned} \chi_{S\to S} &= \frac{p_{S\to S}(\text{high field}) - p_{S\to S}(\text{low field})}{p_{S\to S}(\text{low field})} \\ &= \frac{2}{n(n-1)}. \end{aligned} \tag{17}$$

This suggests that the MFE ought to decrease with n, which is exactly what is found here for systems of related geometry. Practically, as we are going to see below, in systems of diverse mutual reaction possibilities and a symmetric or broken symmetrical configuration, a rich variety of MFEs ensues, which cannot possibly be grasped by the argument presented here. Yet, this discussion provides at least a qualitative description of the origin of the MFEs (in a particular scenario). An analogous analysis can be carried out for a radical pair born in the triplet configuration and recombining as a singlet state. As $p_{T\to S} = \frac{1}{3}(1 - p_{S\to S})$, the singlet probability in low fields is $\frac{1}{4}$ and in high fields

$$p_{T\to S}(\text{high field}) = \frac{1}{4} - \frac{1}{6n(n-1)}. \tag{18}$$

The naïvely predicted MFE is

$$\chi_{T\to S} = -\frac{2}{3n(n-1)}. \tag{19}$$

RESULTS

In this section, we have considered planar systems of up to six radicals with the magnetic field applied perpendicular to the plane of the radicals. While it may seem most natural to consider regular polygons, simplexes, or an evenly spaced linear arrangement (spin chain) when generalizing D3M to more than three radicals, we find that the MFE profiles of such systems can be markedly changed, and often enhanced, with respect to the weak-field sensitivity by the introduction of a small imperfection.

We have considered regular polygons of up to six spins (point group D_{nh}) and linear spin chains of three to six spins. The schematics of the considered geometries and small imperfections introduced into the regular structures are shown in Fig. 1 (polygons) and Fig. 2 (linear chains). The distortions we used were small and enacted upon one spin at a time. An example pertinent to the distortions in regular polygons is the square systems presented in Fig. 1, which differ geometrically only in the position of one spin. We have explored the case of both a small tangential distortion and a radial distortion. The quantity $d = 2R$ is representative of the distance between radicals and was fixed to 15 Å for all but displaced neighboring spins. Similar small distortions were applied to the other polygons studied. The coordinates of all geometries are reported in Sec. S3 of the supplementary material.

With regard to the linear chains, we considered two generic cases: that of a distortion occurring at the end of the chain ($L_{n,n}$ in Fig. 2) and that of a shift in the chain originating at a location within it [$L_{n,m}$ ($m \neq n$) in Fig. 2]. For the latter case, for in-axis displacements, all spins following the displaced radical were likewise rearranged to preserve the inter-spin distances between all but one pair of spins in the chain (in the same way as moving the end spin would affect only one pair, i.e., the terminal spin and its only neighbor). For all distortions, the minimal distance of radicals was $2R$. Within these two generic cases, we considered distortions in each axial direction independently of each other, that is, a distortion along either x, y, or z, the latter of which agrees with the direction of the applied magnetic field.

We begin our analysis by considering the MFEs predicted for the polygonal structures. For the square-geometries of four spins, Fig. 3 shows the MFE on the recombination yield in the singlet state, $\chi_S(B)$, as a function of the applied magnetic field, B, and the exchange interaction J_0. The MFE here is reproduced for the regular square geometry (D_4) and the radial ($D_{4,r}$) and tangential ($D_{n,t}$) distortions. In addition, Fig. 4 shows MFE data for the regular and

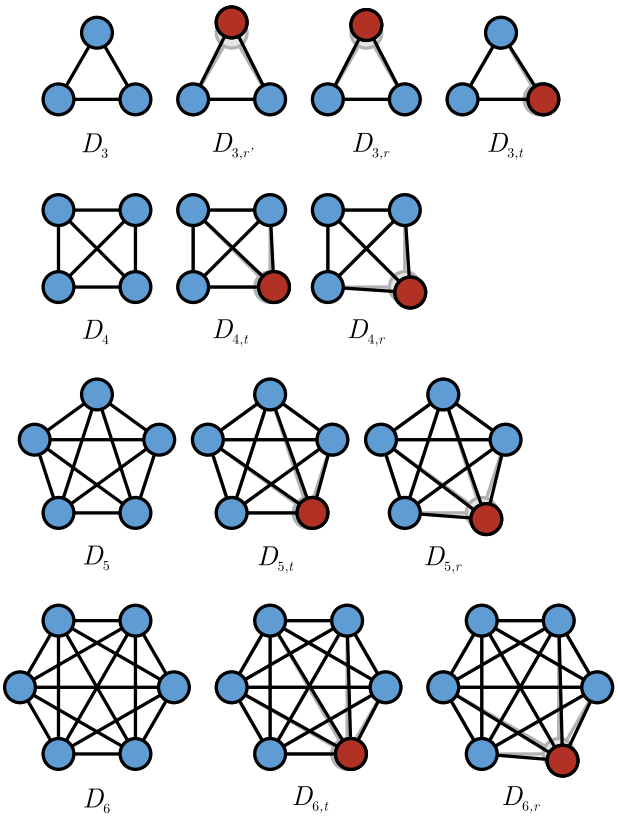

FIG. 1. Schematics of the distortions introduced into the regular polygon geometries. The spins highlighted in red show the areas in which a distortion was applied. The shadowy regions denote the undistorted geometries. The distorted geometries are shown next to the regular geometries (labeled D_n) to illustrate how minor the applied distortions are in comparison with the regular structure, with guiding lines between spin pairs included to highlight subtle changes in the overall symmetry of the shape and thus the interaction parameters in the spin Hamiltonian. In essence, we consider radial and tangential displacements of one spin, indicated by the subscript labels *r* and *t*, respectively. Here, a displacement of 0.05 and 0.1 parts of the inter-spin distance ($2R$) was assumed for the *t* and *r*-variants, respectively. For the triangular geometry, we have considered a smaller radial displacement ($0.1 \times 2R$; $D_{3,r}$) and a larger radial displacement ($0.133 \times 2R$; $D'_{3,r}$).

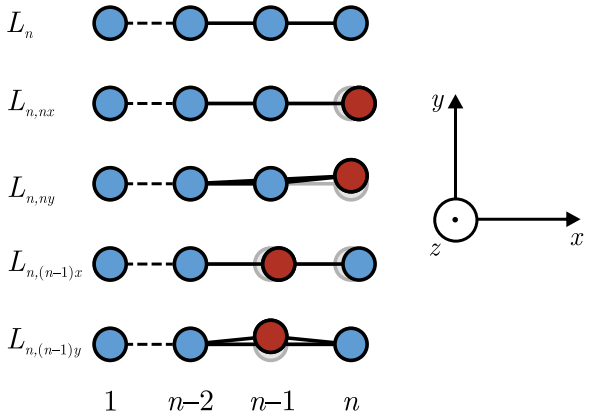

FIG. 2. Schematics of the distortions introduced into the linear chain geometries. The L_n case at the top shows the generic labeling convention for a linear chain of *n* spins, and the spins highlighted in red show the areas in which a distortion was applied. The shadowy regions highlight the difference between the regular and distorted geometries. We consider distortions for which the red spin is displaced perpendicular (labeled *y* and *z*, which are perpendicular and parallel to the applied magnetic field direction) or parallel (*x*) to the spin chain axis. For the *x*-displacements of the *i*th spin, all spins following the *i*th were also displaced in order to maintain the same inter-spin distance of $2R$ for all but the $(i-1, i)$-pair.

radially distorted pentagon. In the supplementary material, we provide similar data for the other geometries, as summarized in Fig. 1. We find that all structures considered exhibit a rich variety of MFEs, whereby the recombination yield is attenuated in high fields. This is in line with the predictions of the naive, qualitative model introduced above, provided that (within this model) the initial state is assumed to be the triplet state of the recombining pair. While the detailed simulations assumed a random initial spin configuration, fast recombination in the singlet state is indeed expected to give rise to spin dynamics resembling that of a triplet-born pair. The detailed calculations also reproduce the naive prediction insofar as the high-field MFEs are decreasing with the increasing number of interacting spins, *n*. Indeed, we find MFEs of up to −0.28, −0.17, −0.11, and −0.06 for the regular polygons with *n* ranging from 3 to 6. What is unexpected though is the behavior upon minor geometrical distortions, as described next.

With reference to Figs. 3 and 4 and the data collected in the supplementary material (see Fig. S2 for the full version of the pentagonal case—abbreviated here for clarity), it is apparent that for the undistorted geometries, e.g., D_4 and D_5, the strongest MFEs are confined to regions of weak exchange and that there are very few regions, if any, of low-field sensitivity. However, applying minor geometrical distortions, such as $D_{4,r}$, $D_{4,t}$, or $D_{5,r}$ in Figs. 3 and 4, we see the emergence of new regions of strong sensitivity to moderate-to-high field intensities at moderate exchange and new regions of weak-field sensitivity. In particular, it is remarkable that the distortions often span new low-field effects below 1 mT and, in part, at field intensities comparable to the Earth's magnetic field and lower, which were completely abolished in the high-symmetry case. What is particularly noteworthy here is that these low-field effects can emerge for comparably strong exchange coupling constants. For the distorted D_5-geometries, e.g., the low-field effects clearly extend beyond the considered window of $|J_0| < 3d_{1,2}$ (see Fig. 4). In higher fields, we likewise find that the primary peak of sensitivity is split to yield several regions of strong moderate-to-high field sensitivity extending to larger, in absolute value, exchange coupling. Taken together, these observations suggest that the distortion grants resilience to the suppressive effects that the exchange interaction usually exerts by energetically decoupling singlet and triplet states. Of further interest is the fact that the effects produced by $D_{n,r}$, $D_{n,t}$, are very different. This suggests that it not only matters *that* axes of symmetry are broken, but *how* this symmetry-breaking occurs. As for the magnitude of the maximal effects, we find that in the majority of cases studied, the maximal $|\chi_S(B)|$ are comparable

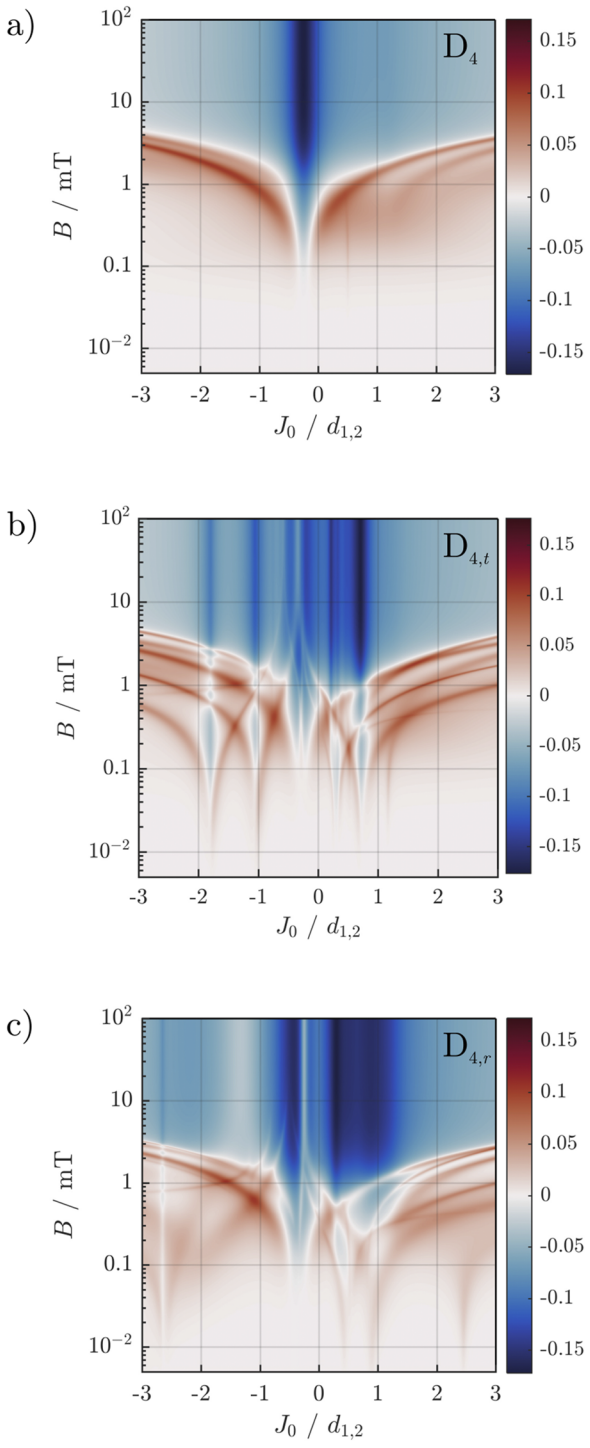

FIG. 3. Heatplots showing the MFE, $\chi_S(B)$ of the square geometries as a function of the exchange coupling parameter J_0 and the magnetic field flux density, B. Panel (a) shows the profile obtained for the perfect square geometry D_4, (b) from distortion $D_{4,t}$, and (c) from $D_{4,r}$. It can be seen that the two distorted geometries show numerous new regions of sensitivity across all magnetic field strengths and exchange interactions studied.

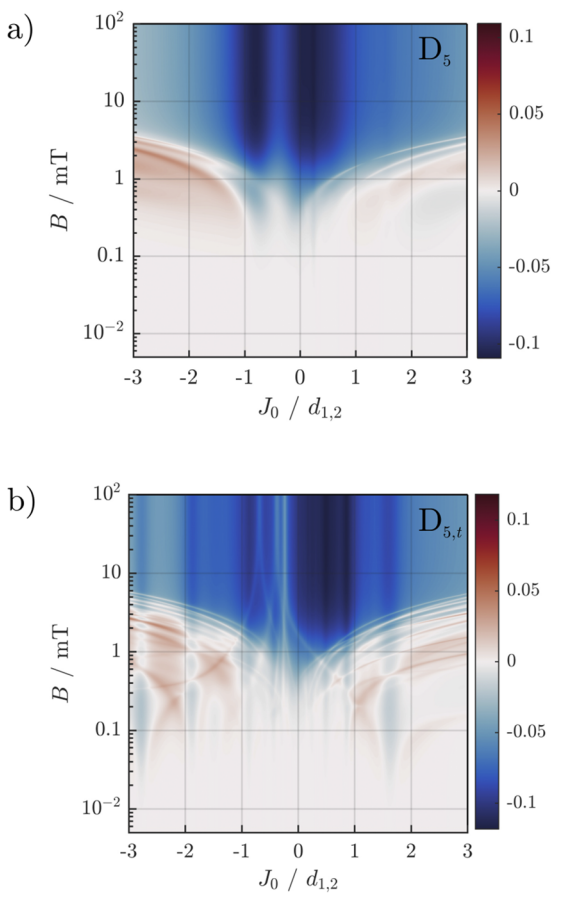

FIG. 4. Heatplots showing the MFE, $\chi_S(B)$ of two pentagonal geometries as a function of the exchange coupling parameter J_0 and the magnetic field flux density, B, pentagonal geometries. Panel (a) shows the profile obtained from the perfect pentagonal geometry D_5 and panel (b) that from $D_{5,t}$. It can be seen that the distorted geometry shows numerous new regions of sensitivity not available in the highly symmetric case.

for distorted and regular geometries. In some cases, however, even minor distortions can somewhat enhance the effect (e.g., for $D_{3,r}$, the maximal absolute MFEs increase from 0.28 to 0.34 employing only a minor radial displacement of 5% of the inter-radical distance; similar effects are seen for the central x-displacements of linear chains; see below).

Similar conclusions can be drawn for the triangular geometry, and larger polygons, in that applying a small distortion and thus breaking some of the axes of symmetry again amplifies the effects at low-field and produces sensitivity to fields of geomagnetic field strength and even lower, at more diverse values of the exchange parameter. See Figs. S1 and S3 of the supplementary material for figures analogous to the presented pentagonal and square cases. See also Figs. S11–S13 of the supplementary material for an illustration that even a radial distortion as small as 0.75 Å is sufficient to produce the effects shown here for 0.75 Å displacements.

We continue our analysis with a discussion of the linear spin chains. Figure 5 shows the recombination yield in the singlet state as a function of the applied magnetic field and the exchange interaction J_0 between pairs of spins in both perfect (evenly spaced) and imperfect variations (see Fig. 2 for illustrations of the nature of the distortions). Data for spin chains of different length, including $n = 3$, are summarized in Figs. S4–S7 of the supplementary material. The latter system has attracted particular interest in the perfect case due to the emergence of a sharp spike of the singlet yield resulting from a level crossing in low magnetic fields.[24] Such spikes in MFE profiles are indicative of a region of high magnetic sensitivity, as could potentially be realized in an optimized quantum navigational device design.

The linear chains share common features that are evident for all n studied. In the symmetric case [exemplified by L_4 in Fig. 5(a)], the MFE is characterized by a sharp feature of positive χ_S for negative J_0, which extends to low-field intensities, and a broad plateau of negative χ_S for positive J_0 and large B. With increasing n, the maximal absolute value of the MFE is reduced (in agreement with the qualitative model from above), the sharp low-field feature of positive χ_S is split into an increasing number of components extending over an increasingly larger range of J_0, and the high-field plateau of negative χ_S broadens. Again, distortions, even if only minor (by less than 10% of the inter-spin distance), can have marked effects on the MFE. For example, $L_{4,3x}$ [Fig. 5(b)] shows an overall amplification of the MFEs relative to the symmetric case, as well as a new region of weak-field sensitivity not accessible for the latter. $L_{4,4x}$ also shows new (but different) areas of weak-field sensitivity, again showing that the particulars of the distortion are actually important to the alterations in the MFE profile. The y-distortions, e.g., $L_{4,4y}$ [see Fig. 5(c)] on the other hand are overall attenuating the MFE but do still produce a new region of sensitivity to moderate-to-high field intensities at strong exchange, thus providing exchange resilience not afforded by the symmetric case. Finally, z-distortions, e.g., $L_{4,3z}$ [Fig. 5(d)], show more subtle effects, the most significant deviation from the symmetric case consisting in the emergence of moderate-intensity weak-field effects at strong exchange. As summarized in the supplementary material, the other linear chains show effects in a similar pattern to that described for L_4 (for a much larger, more comprehensive, version in Fig. 5, see Fig. S5). For example, for $n = 5$ too, the most notable amplifications is provided by the x-distortions, $L_{5,4x}$ and $L_{5,5x}$ (see Fig. S6 of the supplementary material). In general, considering the combined data, we see three effects of small-scale distortions: (a) the onset of MFEs is more pronounced and occurs at more diverse exchange interactions for distorted geometries. (b) Distorted geometries produce new MFEs at high fields. (c) Distorted geometries are more resilient to strong exchange interactions. As for the mechanistic underpinning of the effect, we observe that weak-field MFEs are strongly impacted by quantum level (anti-)crossings as a function of the applied magnetic field. By distorting the geometry, these interactions become more diverse, and in some cases, true crossings become avoided crossings.[24] Such points are the regions of highest sensitivity and are represented as the sharpest regions in the MFE profile of a system. For a qualitative illustration of how level crossings are influenced, see Fig. S10 of the supplementary material. We also provide qualitative discussions of the mechanistic origin of the enhancing effect of small distortions in Sec. S2 of the supplementary material.

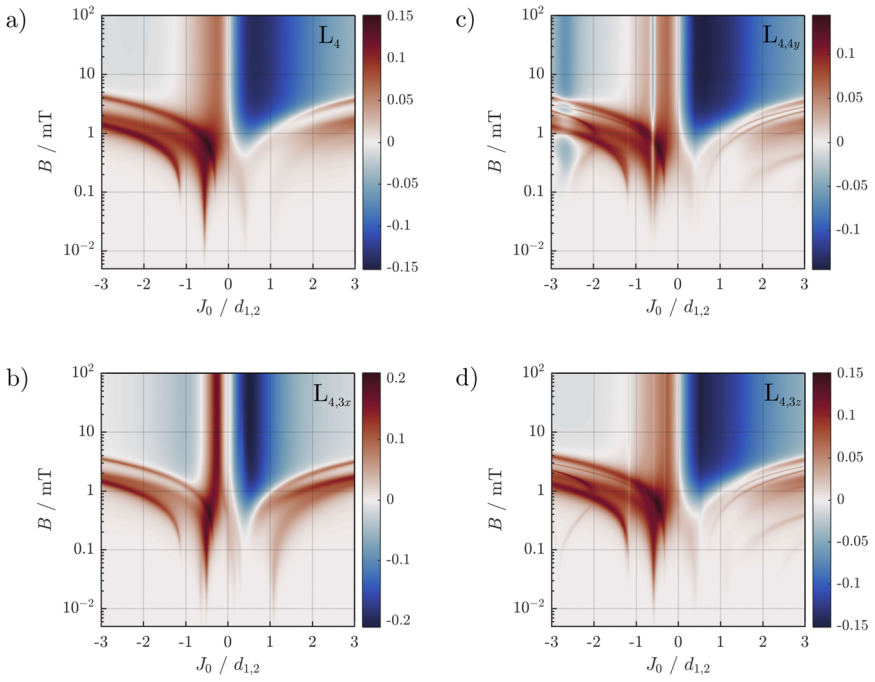

FIG. 5. MFE profiles, i.e., χ_S as a function of J_0 and B, obtained from distorting the four-spin linear geometry. Panel (a) shows the control case of the evenly spaced chain, L_4. Panels (b)–(d) show the distortions $L_{4,3x}$, $L_{4,4y}$, and $L_{4,3z}$, respectively.

In order to quantitatively capture the observations qualitatively summarized above, we introduce a new measure $M(B)$, defined by

$$M(B) = \frac{1}{\Delta J} \int |\chi_S(B,J)|_{\text{dist}} - |\chi_S(B,J)|_{\text{per}} dJ, \tag{20}$$

where $|\chi_S(B, J)|_{\text{dist}}$ is the absolute value of the MFE at a particular value of field B of the distorted geometry and $|\chi_S(B, J)|_{\text{per}}$ is the same quantity for the perfect geometry. ΔJ is the range of exchange values that the integral is evaluated for; we use the same exchange region as used in the density plots above, i.e., J_0 ranging from $-3d_{1,2}$ to $3d_{1,2}$ and, thus, $\Delta J = 6d_{1,2}$. A positive value of $M(B)$ indicates that at the magnetic field B, on the average, the MFE is enhanced by the distortion for the considered range of exchange interactions.

We have evaluated $M(B)$ for the analyzed geometries (using the Simpson quadrature). The results are shown in Fig. 6. In this figure, we can see that $M(B)$ is almost always positive for weak to moderate magnetic fields, showing the improvement that geometric distortions can give. For weak fields—in particular around the Earth's magnetic field intensity—the distorted geometry almost always outperforms the perfect geometry. The one exception to this pattern is the distortion in the y-direction for the special case of the linear geometry, which is overall detrimental to the weak-field MFEs. In general for the linear geometries, one can see that $M(B)$ is strongly positive for distortions in the x-direction and slightly positive for those in the z-direction across all field intensities. For the regular polygons, weak field and high-field results are generally positive, showing the distorted geometry outperforming the perfect geometry. Results are mixed for moderate field intensities, being the triangular geometry's most impressive region of amplification, but an area where the square and pentagonal measures are negative before returning to positivity at the high field; the hexagonal measure is positive everywhere. The fact that the measures for the different distortions of the same individual geometries are so varied is further evidence that it is not only the breaking of the symmetry that matters to the magnetosensitivity of a spin system but also *how* the symmetry is broken. Note furthermore that extending the integral to a larger J_0-range would give a larger $M(B)$ for many of the cases studied.

With this new measure, we note that the distorted triangle is a particularly impressive case, with the distortion reducing the minimum field required to see a strong effect by a factor of 10 (see Tables S1 and S2 of the supplementary material) and producing an Earth-strength MFE where previously this was forbidden by the symmetry.

DISCUSSION OF ROBUSTNESS OF THE RESULTS PRESENTED

Here, we focus on structures that have distorted, non-symmetric equilibrium structures that preserve a degree of asymmetry. In many scenarios, e.g., the radially distorted hexagon, the enhancing effect can be observed for displacements both in the positive and negative radial direction. This is, e.g., for $D_{4,r}$ and $D_{6,r}$, shown in Fig. S14 of the supplementary material. Therefore, the effect presented here is expected to survive if the system comprises ensembles of structures with various, i.e., both positive and negative, displacements if the interconversion between such structures is slow on the spin-dynamics timescale. If, on the other hand, fast (e.g., vibrational) dynamics realize an average undistorted system

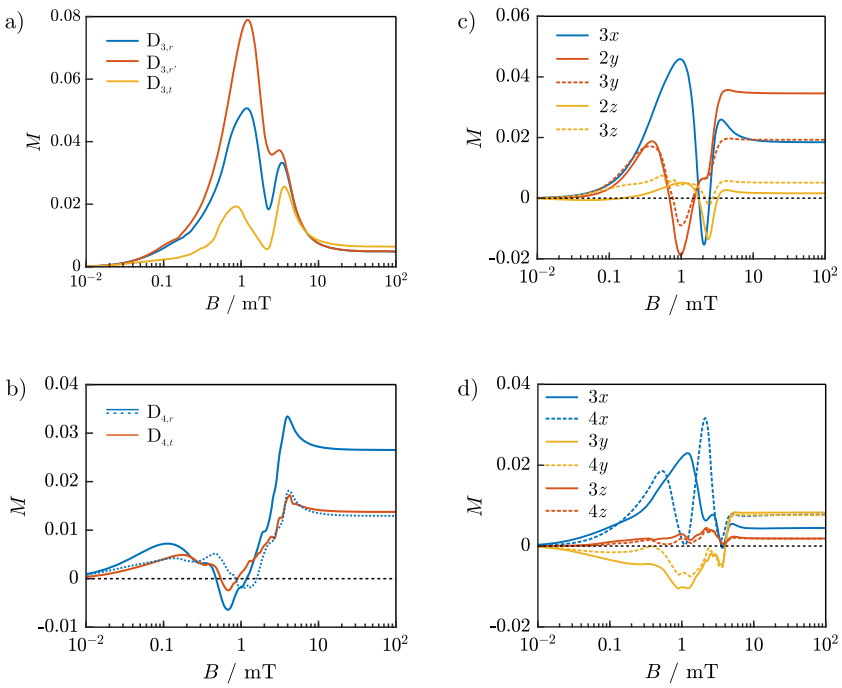

FIG. 6. Enhancement measures $M(B)$, calculated using the perfect geometry as the reference value, shown for the distorted triangle (a) and square geometry (b) and the linear chain systems with $n = 3$ and $n = 4$ [(c) and (d)]. For (b), we show data for the radial displacement of one spin by 1.5 Å (blue solid line) and 0.75 Å (blue dotted line) and the tangential displacement by 0.75 Å (red solid line). For the linear chains, the displacement was 1.5 Å applied as laid out in Fig. 2. Data for the other geometries studied are collected in Figs. S8 and S9 of the supplementary material.

on a timescale faster than the spin dynamics, then, trivially, it is the latter that dictates the spin dynamics and D*n*M applies in its symmetric form. The motion of radicals on a timescale comparable to the spin dynamics is clearly an important question, which is, however, beyond this work.

Figure 6(a) shows the effect of two radial distortions to a different extent. To ensure the robustness of our conclusions, we have further undertaken a systematic evaluation, which we summarize in Figs S14 and S15 of the supplementary material. For a lifetime of the radical pair on the order of 1 μs, the dynamics are expected to be sensitive to changes of the eigenvalues of the Hamiltonian of the order of 1 MHz.[30] As for the typical inter-radical distances here, an increase of the distance by 0.34 Å gives rise to a change in the dipolar coupling constant $d_{i,j}$ of 1 MHz, distortions of at least a few tenths of Angstroms are necessary to elicit a significant effect (see Fig. S14 of the supplementary material). Larger displacements may or may not give rise to a decrease in the MFE depending on the properties of the "remaining" spin system. However, as this is essentially a different system, a general assessment is not possible.

In addition, we have shown that random displacements of several spins likewise preserve the enhancing effect deduced for the displacement of a single spin. In particular, the average enhancement measure of an ensemble of randomly distorted 4-spin systems is shown in Fig. S15 of the supplementary material, which is qualitatively the same as for the radical or tangential distortion of a single spin location shown in Fig. 6(b). We therefore conclude that the effect is not peculiar to the selected distortions, as summarized in Figs. 1 and 2, but applies more generally. This conclusion is further corroborated by the distance dependence of the enhancement, as shown in Fig. S14.

GENERAL DISCUSSION

Symmetry is central to nature. It is also essential to many branches of science because the discovery (or imposition) of certain symmetries upon a system of interest can serve to dramatically simplify the theoretical analysis. Thus, symmetry is often the first port of call when tackling daunting problems, and indeed many such problems are considered only in special, high-symmetry, formulations due to the analytical/computational intractability of the general case. This also applies to the spin dynamics of systems of radicals, which often requires a high level of abstraction and/or symmetry to be tractable.[31–34]

Although symmetry can be a powerful tool, the breaking of symmetry can produce new and often interesting results. *Spontaneous* symmetry-breaking is a widely known phenomenon, observed, e.g., the Ginzburg–Landau theory of phase transitions, systems described by the so-called "Mexican hat" potential, the Jahn–Teller effect, and indeed present even in many everyday situations.[35–37]

Examples of semiconductor quantum devices[38] show how technological applications, e.g., in sensing, can be revolutionized by deliberately breaking symmetries, and our work reported here suggests that similar principles might apply for magnetic *sensing* as it, e.g., pertains to biological MFEs or more generally to spin chemical phenomena.[15,39] In particular, we argue that a natural symmetry absence may go some way to explaining the remarkable sensitivity of these systems to weak magnetic fields, and also how such effects can be sustained under realistic scenarios involving, e.g., large exchange coupling.

MFEs that originate from the coherent dynamics of more than two radicals are a new topic of interest. These have been supposed to enhance the magnetosensitivity of the lipid peroxidation and the directionality in the cryptochrome compass for which preliminary theoretical results have been obtained.[27] It is not inconceivable that the mechanism could apply broadly, in isolation or in combination with hyperfine-driven intersystem crossing, to many scenarios of MFEs in biological systems for which the EED interaction is typically not averaged by motion due to the reduced mobility of radicals or radicals being parts of larger, ordered compounds and for which radicals are sometimes plentiful. While highly symmetric structures of *n* radicals are at this stage of study a logical extension of the previously explored model, it is surprising to realize that virtue in fact lies in imperfection. One would expect that the geometries from random encounters of radicals as well as the average biological structure are much more likely to be distorted than regular, suggesting that our finding adds an important piece to the puzzle of understanding biological magnetosensitivity, where imperfect geometries are statistically far more likely to arise than perfect order.

We have shown in a previous work that the re-introduction of hyperfine interactions does not significantly dampen *DnM* magnetic field effects if the dipolar interaction is the dominant term of the spin Hamiltonian, and so we are confident that all effects shown here would persist in the presence of coupled nuclei.[27]

It is obvious that the simulations described here describe scenarios that are difficult to realize in practice. Obviously, aligning six spins in a perfect hexagonal arrangement to then undergo reactive quantum spin dynamics might be difficult to actualize. However, considering one pair of radicals to be in an initial singlet state (between which $d_{1,2}$ would be defined) in the presence of other, stable radicals acting as an external "bath" is not unrealistic. One way to realize this chemically would be to generate radical pairs in the presence of more stable radicals. As soon as the constraint upon perfection (symmetry) is removed, the practicality of realization increases significantly and indeed may even occur naturally or at random. Though we do not consider this particular scenario in the present work, it would be a way to build up the kind of configuration we explored. We hope that this motivates more experimental research into this idea.

It is interesting to note that the MFEs in radical pairs and dipolarly coupled *n*-spin systems can also be viewed a result of the absence of symmetry in their own right. The missing symmetry here is a permutation symmetry of two electron spins poised to recombine to form a diamagnetic state.[24] In the conventional radical pair mechanism, this symmetry is broken by hyperfine interactions with magnetic nuclei. In D3M, this asymmetry is provided by the electron–electron dipolar interaction in systems of more than two radicals. In this sense, for both scenarios remarkable, MFEs can result from this natural symmetry absence.

Practically, the amplifications observed here could also be used to make quantum devices more sensitive, easier to make, and easier to control. Quantum devices made using the principles of this mechanism would not be subject to a precise positional confinement of the reacting radicals, and so small distortions would work to the

advantage of the engineer. Such devices would be more sensitive due to the extra features available in the MFE profiles that, as we have illustrated in this work, appear when a system's geometric equilibrium is removed. The effects could furthermore be optimized by tuning the exchange interaction and moving the anti-crossings responsible for the MFE spikes to lower field values, thereby realizing optimal sensitivity at the projected field intensity.

CONCLUSION

We here have introduced the mechanism, D*n*M, for an abstract scenario and tried to elucidate some of its properties. D*n*M treats the oft-neglected electron–electron dipolar interaction as the main contributor to MFEs rather than the conventionally used hyperfine interaction. This mechanism thus applies to radicals without dominant hyperfine interactions but can impact the spin dynamics in classical radical pair systems with non-negligible hyperfine and/or exchange interactions, as recently demonstrated for lipid peroxidation and the avian compass. This interaction pattern of three or more radicals thus provides a robust additional mechanism for radical systems at concentrations for which multi-radical correlations cannot be neglected. Here, we have explored the possibility of this mechanism for systems comprising more than the previously considered three radicals. We have demonstrated that a rich variety of magnetosensitivity can, in principle, ensue for *n*-radical systems coupled by the long-range electron–electron dipolar interaction. We have further explored these effects in configurations that are more statistically likely to occur in nature by comparing the perfect theoretical systems of regular geometries with slightly distorted geometries that break various rotation and reflection symmetries. In the large majority of cases considered, such imperfections have enhanced the magneto-sensitivity. In particular, we have observed increasing sensitivity to weak magnetic fields for the selected values of the exchange parameter and an increase in the number, and range, of exchange parameters for which low-field sensitivity manifests.

These findings are important because they further suggest that the D3M model and its generalization discussed here, D*n*M, can provide large magnetosensitivity in a variety of circumstances. The prediction of new MFEs in such systems allows the consideration of processes and conditions that had previously been thought impossible due to the constraints of the RPM and further inspires experimental endeavors into the study of magnetic field effects in ordered systems and at high radical concentrations or the production of devices that utilize *n*-spin processes as a measuring tool. Here, many questions about realizability remain open. However, it is not our aim to guide future experiments yet but to instigate the principal possibility to observe magnetic field effects in radical recombination reactions due to the electron–electron dipolar interaction alone of three or more radicals and to highlight that imposing perfect geometries might reduce the sensitivity toward weak magnetic fields.

While the mechanism has been presented in abstract terms, we think that real-world scenarios that involve the aspects of the model as laid out here are not inconceivable. We speculate that the effect could play a role in lipid peroxidation of membranes where, e.g., for the L_o phase, local hexagonal packings could realize transient encounters of peroxyl radicals that resemble the scenario described.[40] As the lateral diffusion is slow, these systems would resemble immobilized and, naturally, distorted geometries on the time scale of the spin dynamics.[27] Furthermore, the model could apply with small adjustments to recombination reactions of pairs of radicals generated in an environment of radicals. This could, e.g., be relevant in the context of arrays of cryptochrome sensors, which form long-lived radicals following their magnetosensitive photoactivation. Here, the question arises whether the crosstalk of cryptochrome radical pairs and adjacent, more persistent radicals could play a role either adversely or possibly even as an enhancing factor. Other applications could be found in the context of organic spintronic materials and devices,[41] where asymmetry could be introduced via lattice defects. Here, effects beyond the bipolaron picture can be expected for large charge carrier densities. While the model here is abstract, it paves the path to addressing these and related questions in a concrete context.

SUPPLEMENTARY MATERIAL

See the supplementary material for additional data on the magnetic field dependence of the recombination yield of distorted and undistorted structures, data in support of the robustness of the claim that symmetry distortion can boost the magnetosensitivity, exemplary level crossing-diagrams, and a qualitative discussion of the mechanistic underpinning.

ACKNOWLEDGMENTS

We gladly acknowledge the use of the University of Exeter High-Performance Computing facility in carrying out this work and the EPSRC (Grant No. EP/R021058/1) for financial support.

DATA AVAILABILITY

The data that support the findings of this study are available from the corresponding author upon reasonable request.

REFERENCES

[1] U. E. Steiner and T. Ulrich, Chem. Rev. **89**, 51 (1989).
[2] K. M. Salikhov, Y. N. Molin, R. Sagdeev, and A. Buchachenko, *Spin Polarization and Magnetic Effects in Radical Reactions, Vol. 22 of Studies in Physical and Theoretical Chemistry* (Elsevier, Amsterdam, 1984).
[3] K. A. McLauchlan and U. E. Steiner, Mol. Phys. **73**, 241 (1991).
[4] H. Hayashi, *Introduction to Dynamic Spin Chemistry: Magnetic Field Effects on Chemical and Biochemical Reactions* (World Scientific Publishing Company, 2004), Vol. 8.
[5] I. R. Gould, N. J. Turro, and M. B. Zimmt, *Advances in Physical Organic Chemistry* (Elsevier, 1984), Vol. 20, pp. 1–53.
[6] E. W. Evans, D. R. Kattnig, K. B. Henbest, P. J. Hore, S. R. Mackenzie, and C. R. Timmel, J. Phys. Chem. **145**, 085101 (2016).
[7] D. R. Kattnig, E. W. Evans, V. Déjean, C. A. Dodson, M. I. Wallace, S. R. Mackenzie, C. R. Timmel, and P. J. Hore, Nat. Chem. **8**, 384 (2016).
[8] K. Maeda, K. B. Henbest, F. Cintolesi, I. Kuprov, C. T. Rodgers, P. A. Liddell, D. Gust, C. R. Timmel, and P. J. Hore, Nature **453**, 387 (2008).
[9] K. Schulten, C. E. Swenberg, and A. Weller, Z. Phys. Chem. **111**, 1 (1978).
[10] P. J. Hore and H. Mouritsen, Annu. Rev. Biophys. **45**, 299 (2016).

[11] N. Lambert, Y.-N. Chen, Y.-C. Cheng, C.-M. Li, G.-Y. Chen, and F. Nori, Nat. Phys. **9**, 10 (2013).
[12] J. McFadden and J. Al-Khalili, Proc. R. Soc. London, Ser. A **474**, 20180674 (2018).
[13] A. L. Buchachenko and V. L. Berdinsky, J. Phys. Chem. **100**, 18292 (1996).
[14] A. S. Letuta and V. L. Berdinskii, Dokl. Phys. Chem. **463**, 179 (2015).
[15] D. R. Kattnig, J. Phys. Chem. B **121**, 10215 (2017).
[16] K. M. Salikhov, J. H. Golbeck, and D. Stehlik, Appl. Magn. Reson. **31**, 237 (2007).
[17] V. I. Borovkov, I. S. Ivanishko, V. A. Bagryansky, and Y. N. Molin, J. Phys. Chem. A **117**, 1692 (2013).
[18] I. M. Magin, P. A. Purtov, A. I. Kruppa, and T. V. Leshina, Appl. Magn. Reson. **26**, 155 (2004).
[19] I. M. Magin, P. A. Purtov, A. I. Kruppa, and T. V. Leshina, J. Phys. Chem. A **109**, 7396 (2005).
[20] P. J. Hore, D. A. Hunter, F. G. H. van Wijk, T. J. Schaafsma, and A. J. Hoff, Biochim. Biophys. Acta Bioenerg. **936**, 249 (1988).
[21] S. Yeganeh, M. R. Wasielewski, and M. A. Ratner, J. Am. Chem. Soc. **131**, 2268 (2009).
[22] B. K. Rugg, M. D. Krzyaniak, B. T. Phelan, M. A. Ratner, R. M. Young, and M. R. Wasielewski, Nat. Chem. **11**, 981 (2019).
[23] D. R. Kattnig and P. Hore, Sci. Rep. **7**, 11640 (2017).
[24] R. H. Keens, S. Bedkihal, and D. R. Kattnig, Phys. Rev. Lett. **121**, 096001 (2018).
[25] N. S. Babcock and D. R. Kattnig, J. Phys. Chem. Lett. **11**, 2414 (2020).
[26] O. Efimova and P. J. Hore, Biophys. J. **94**, 1565 (2008).
[27] C. Sampson, R. H. Keens, and D. R. Kattnig, Phys. Chem. Chem. Phys. **21**, 13526 (2019).
[28] R. Haberkorn, Mol. Phys. **32**, 1491 (1976).
[29] R. H. Keens and D. R. Kattnig, New J. Phys. **22**, 083064 (2020).
[30] H. G. Hiscock, S. Worster, D. R. Kattnig, C. Steers, Y. Jin, D. E. Manolopoulos, H. Mouritsen, and P. J. Hore, Proc. Natl. Acad. Sci. U. S. A. **113**, 4634 (2016).
[31] C. R. Timmel, U. Till, B. Brocklehurst, K. A. Mclauchlan, and P. J. Hore, Mol. Phys. **95**, 71 (1998).
[32] E. M. Gauger, E. Rieper, J. Morton, S. C. Benjamin, and V. Vedral, Phys. Rev. Lett. **106**(4), 040503 (2011).
[33] L. P. Lindoy and D. E. Manolopoulos, Phys. Rev. Lett. **120**, 220604 (2018).
[34] D. E. Manolopoulos and P. J. Hore, J. Phys. Chem. **139**, 124106 (2013).
[35] J. Shaver, J. Kono, O. Portugall, V. Krstić, G. L. J. A. Rikken, Y. Miyauchi, S. Maruyama, and V. Perebeinos, Nano Lett. **7**, 1851 (2007).
[36] B. Rosenstein and D. Li, Rev. Mod. Phys. **82**, 109 (2010).
[37] J. J. Frost, K. J. Pienta, and D. S. Coffey, Oncotarget **9**, 11429 (2018).
[38] M. E. Portnoi, M. Rosenau da Costa, O. V. Kibis, and I. A. Shelykh, Int. J. Mod. Phys. B **23**, 2846 (2009).
[39] D. R. Kattnig, I. A. Solov'yov, and P. J. Hore, Phys. Chem. Chem. Phys. **18**, 12443 (2016).
[40] A. J. Sodt, M. L. Sandar, K. Gawrisch, R. W. Pastor, and E. Lyman, J. Am. Chem. Soc. **136**, 725 (2014).
[41] R. Geng, T. T. Daugherty, K. Do, H. M. Luong, and T. D. Nguyen, J. Sci.: Adv. Mater. Devices **1**, 128 (2016).